
Article

Not peer-reviewed version

Multilayer Epitaxial Heterostructures With Multi-Component III-V:Fe Magnetic Semiconductors

Alexey V. Kudrin , Valeri P. Lesnikov , [Ruslan N. Kriukov](#) , Yuri A. Danilov , [Mikhail V. Dorokhin](#) ,
Anastasia A. Yakovleva , [Nataliya Yu. Tabachkova](#) , [Nikolai A. Sobolev](#) *

Posted Date: 31 July 2023

doi: [10.20944/preprints202307.2049.v1](https://doi.org/10.20944/preprints202307.2049.v1)

Keywords: magnetic semiconductors; pulsed laser deposition; III-V heterostructures; transmission electron microscopy; x-ray photoelectron spectroscopy; magnetoresistance



Preprints.org is a free multidiscipline platform providing preprint service that is dedicated to making early versions of research outputs permanently available and citable. Preprints posted at Preprints.org appear in Web of Science, Crossref, Google Scholar, Scilit, Europe PMC.

Copyright: This is an open access article distributed under the Creative Commons Attribution License which permits unrestricted use, distribution, and reproduction in any medium, provided the original work is properly cited.

Article

Multilayer Epitaxial Heterostructures with Multi-Component III–V:Fe Magnetic Semiconductors

A.V. Kudrin ¹, V.P. Lesnikov ¹, R.N. Kriukov ¹, Yu.A. Danilov ¹, M.V. Dorokhin ¹, A.A. Yakovleva ¹, N.Yu. Tabachkova ^{2,3} and N.A. Sobolev ^{4,5,*}

¹ Lobachevsky State University of Nizhny Novgorod, Gagarin av. 23/3, 603950 Nizhny Novgorod, Russia;

² Department of Materials Science of Semiconductors and Dielectrics, National University of Science and Technology "MISiS", 119049 Moscow, Russia;

³ Prokhorov General Physics Institute, Russian Academy of Sciences, 38 Vavilov st., 119991 Moscow, Russia;

⁴ Department of Physics and i3N, University of Aveiro, 3810-193 Aveiro, Portugal;

⁵ Laboratory of Functional Low-dimensional Structures, National University of Science and Technology "MISiS", 119049 Moscow, Russia;

* Correspondence: sobolev@ua.pt; Tel.: +351 234 378 117

Abstract: Three-layer structures based on various multi-component films of III–V semiconductors heavily doped with Fe were grown by pulsed laser sputtering of InSb, GaSb, InAs, GaAs and Fe solid targets. The structures comprising InAsSb:Fe, InGaSb:Fe and InSb:Fe layers with Fe concentrations up to 24 at. % separated by GaAs spacers were deposited on (001) i-GaAs substrates at 200°C. Transmission electron microscopy showed that the structures have a rather high crystalline quality and do not contain secondary-phase inclusions. X-ray photoelectron spectroscopy investigations revealed significant diffusion of Ga atoms from the GaAs regions into the InAsSb:Fe layers, which has led to the formation of an InGaAsSb:Fe compound with a Ga content up to 20 at. %. It has been found that the ferromagnetic properties of the InAsSb:Fe magnetic semiconductor improve with increasing Sb:As ratio. It has been concluded that the indirect ferromagnetic exchange interaction between Fe atoms occurs predominantly via Sb atoms.

Keywords: magnetic semiconductors; pulsed laser deposition; III–V heterostructures; transmission electron microscopy; X-ray photoelectron spectroscopy; magnetoresistance

1. Introduction

III–V semiconductors heavily doped with iron atoms are of interest for semiconductor spintronics as well as for solid-state physics in general since they exhibit pronounced ferromagnetic properties up to room temperature. In particular, (Ga,Fe)Sb [1,2], (In,Fe)Sb [3,4], GaAs:Fe [5] epitaxial layers with concentrations of Fe atoms up to 20 at. % and Curie temperatures above 300 K were obtained by molecular beam epitaxy and/or pulsed laser deposition (PLD). Despite the very high Fe doping level, these layers are single-phase ferromagnetic semiconductors with the intrinsic mechanism of ferromagnetic ordering. The III–V:Fe magnetic semiconductors can be either n-type ((In,Fe)As, (In,Fe)Sb, GaAs:Fe) or p-type (Ga,Fe)Sb, which is necessary for the implementation of bipolar spintronic devices. In particular, this makes it possible to create n-p diode structures with two III–V:Fe magnetic semiconductor layers of different conductivity types, such as (Ga,Fe)Sb and (In,Fe)Sb [6,7] as well as (Ga,Fe)Sb and (In,Fe)As [7]. It is also possible to form ferromagnetic layers based on heavily Fe-doped III–V multi-component semiconductor solid solutions. In particular, Fe-doped ferromagnetic layers based on a $In_{1-x}Ga_xSb$ matrix were obtained [8]. The interest in multi-component III–V:Fe magnetic semiconductor solid solutions stems from the unique possibilities of manipulating the basic semiconductor parameters (type of majority charge carriers, band gap and crystal lattice parameters) by varying the composition of the III–V matrix. This will potentially expand the use of the III–V:Fe magnetic semiconductors towards the creation of semiconductor spintronic devices. In this work, we present the results of the fabrication of three-layer

heterostructures with III–V:Fe magnetic semiconductor layers based on the $\text{In}_{1-x}\text{Ga}_x\text{Sb}$ and $\text{InAs}_{1-x}\text{Sb}_x$ solid solutions.

2. Materials and Methods

The structures presented in this work were grown on semi-insulating (001) GaAs substrates by pulsed laser sputtering of InSb, GaSb, InAs, GaAs and Fe solid targets in a vacuum [2,3]. The nominal composition of the formed layers was set by the ratio of the target sputtering times. To form the InAsSb:Fe layers, the cyclic serial sputtering of the InAs, InSb and Fe targets was carried out. The InGaSb:Fe layers were formed using the InSb, GaSb and Fe targets. The temperature of the growth process for all structures was 200 °C since this temperature was earlier found to be optimal for the growth of III–V:Fe magnetic semiconductors by PLD [3,5,6]. The structural properties of the fabricated samples were investigated by high-resolution transmission electron microscopy (HRTEM). The composition of the structures was studied by X-ray photoelectron spectroscopy (XPS). The concentration of elements was determined using relative sensitivity factors [9]. The absolute error in the determination of the atom concentration in the used XPS method is 1 at. %. Magnetotransport measurements were carried out in the van der Pauw geometry in a closed-cycle He cryostat.

3. Results

3.1. Three-layer structures

Three types of three-layer structures containing two III–V:Fe layers separated by a GaAs spacer were formed and studied:

Sample M1 – an $\text{InAs}_{0.5}\text{Sb}_{0.5}\text{Fe}$ and an $\text{InAs}_{0.8}\text{Sb}_{0.2}\text{Fe}$ layer separated by an undoped GaAs layer. The nominal Fe concentration was set equal to 17 at. %.

Sample M2 – an $\text{InAs}_{0.5}\text{Sb}_{0.5}\text{Fe}$ and an $\text{In}_{0.2}\text{Ga}_{0.8}\text{Sb}\text{Fe}$ layer separated by an undoped GaAs layer. The nominal Fe concentration was set equal to 17 % and 20 at. % for the $\text{InAs}_{0.5}\text{Sb}_{0.5}\text{Fe}$ and $\text{In}_{0.2}\text{Ga}_{0.8}\text{Sb}\text{Fe}$ layers, respectively.

Sample M3 – an $\text{In}_{0.2}\text{Ga}_{0.8}\text{Sb}\text{Fe}$ and an InSb:Fe layer separated by an undoped GaAs layer. The nominal Fe concentration was set equal to 20 at. %.

The nominal thickness of each layer was set equal to 25 nm. The structures are listed in Table 1.

Table 1. The investigated three-layered samples and their nominal composition.

Sample	Structure
M1	$(\text{InAs}_{0.8}\text{Sb}_{0.2})_{0.83}\text{Fe}_{0.17}/\text{GaAs}/(\text{InAs}_{0.5}\text{Sb}_{0.5})_{0.83}\text{Fe}_{0.17}/i\text{-GaAs substrate}$
M2	$(\text{In}_{0.2}\text{Ga}_{0.8}\text{Sb})_{0.8}\text{Fe}_{0.2}/\text{GaAs}/(\text{InAs}_{0.5}\text{Sb}_{0.5})_{0.83}\text{Fe}_{0.17}/i\text{-GaAs substrate}$
M3	$(\text{InSb})_{0.8}\text{Fe}_{0.2}/\text{GaAs}/(\text{In}_{0.2}\text{Ga}_{0.8}\text{Sb})_{0.8}\text{Fe}_{0.2}/i\text{-GaAs substrate}$

Figure 1(a) shows an overview cross-section TEM image and Figure 1(b) shows an HRTEM image of sample M1. The images clearly reveal all grown layers: the lower (closest to the substrate) InAsSb:Fe layer (ca. 33 nm thick), the GaAs spacer layer (ca. 29 nm thick) and the upper InAsSb:Fe layer (ca. 25 nm thick). All three deposited layers are flat and epitaxial. No secondary phase inclusions were observed (they may be visualized in III–V:Fe layers in the form of regions with a moiré-type contrast [6]). The images reveal the presence of microtwins which appear in the form of straight lines at an angle of ca. 70° with respect to each other. The microtwins are typical crystal defects for the formed layers due to the large lattice mismatch between the InAsSb and GaAs crystals. The inset of Figure 1(b) shows a fast Fourier transform (FFT) diffraction pattern of the whole HRTEM image. The pattern contains spots corresponding to a zinc-blende-type crystal structure for the GaAs (substrate and intermediate layer) and InAsSb:Fe regions. The diffraction spots located at a smaller distance from the central spot in the reciprocal space (the inner spots denoted as MS – magnetic

semiconductor) correspond to the InAsSb:Fe layers with a larger lattice parameter, while the spots with a larger distance correspond to the GaAs regions with a smaller lattice parameter.

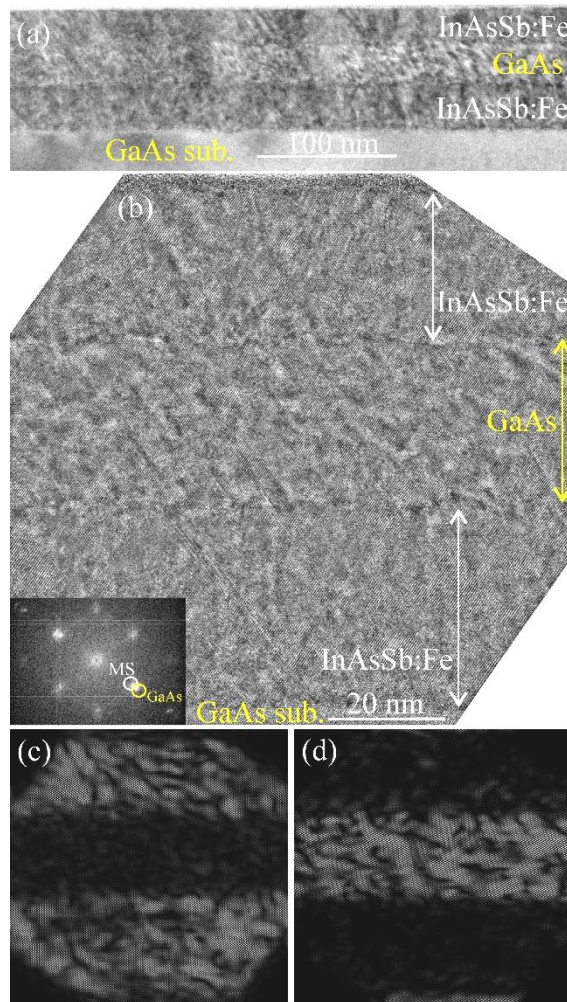


Figure 1. Cross-section TEM images of the InAsSb:Fe/GaAs/InAsSb:Fe/GaAs(sub.) sample M1. (a) Overview TEM image. (b) HRTEM image. The inset shows the respective FFT diffraction pattern. (c) Inverse FFT image of the Fe-doped regions obtained from MS spots. (d) Inverse FFT image of the GaAs regions obtained from GaAs spots.

Figures 1(c) and 1(d) exhibit inverse FFT images obtained from the MS and GaAs spots of the FFT diffraction pattern. The images clearly show that the GaAs regions and the InAsSb:Fe layers have different lattice parameters, and the lattice parameter of the GaAs spacer is close to the lattice parameter of the GaAs substrate. It should be noted that the change in the lattice parameter (layer relaxation) occurs in a very thin region (a few nanometers thick). The analysis of the HRTEM image shows that the lattice parameter of the lower InAsSb:Fe layer is larger than that of the GaAs spacer by ca. 13 %. At the same time, the lattice parameter of the upper InAsSb:Fe layer is larger than that of the GaAs spacer by ca. 8 %. This result agrees with the nominal composition of the InAsSb:Fe layers (Table 1), since the lower InAsSb:Fe layer contains a higher concentration of Sb in the InAsSb semiconductor matrix than the upper InAsSb:Fe layer. Note that the lattice mismatch between GaAs and InSb amounts to 14.6 % and between GaAs and InAs to 7.2 %.

Figure 2 shows cross-section HRTEM images of sample M1 obtained at a higher magnification in the region of the lower InAsSb:Fe layer (a), in the region of the GaAs spacer (b) and in the region of the upper InAsSb:Fe layer (c). It can be seen from the HRTEM images that all layers possess a fairly high crystalline quality and do not contain inclusions with a crystal lattice different from the zinc-blende type.

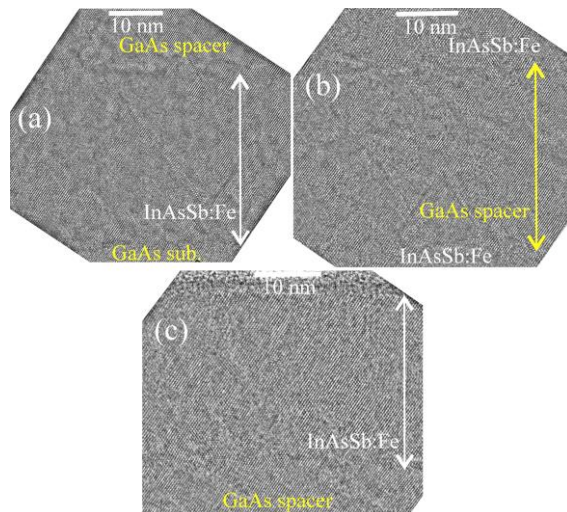


Figure 2. Cross-section HRTEM images of the layers of sample M1. (a) HRTEM image of the lower InAsSb:Fe layer. (b) HRTEM image of the GaAs spacer. (c) HRTEM image of the upper InAsSb:Fe layer.

Figure 3 exhibits XPS dependences of the concentration of C, O, In, Ga, As, Sb and Fe atoms on the distance from the surface for sample M1. The Fe concentration in the InAsSb:Fe layers detected by XPS equals about 13–14 at. %, which is consistent with the nominal Fe concentration (17 at. %). The lower InAsSb:Fe layer has an Sb concentration approximately three times higher than that of the upper InAsSb:Fe layer, which is also in agreement with the technological parameters of the layers (Table 1). It is noteworthy that the layers with the nominal composition of InAsSb:Fe contain a significant concentration of Ga atoms (no less than 12 at. % in the lower layer and no less than 4 at. % in the upper layer) although Ga was not introduced during the growth of these layers. The presence of Ga in these layers is apparently related to Ga diffusion from the GaAs substrate and spacer during the growth process. Actually, the formed magnetic semiconductor films are layers of the InGaAsSb quaternary solid solution heavily doped with Fe. It is also seen from the XPS profiles that Fe atoms tend to diffuse towards the direction opposite to the growth direction (towards the substrate) despite the relatively low temperature of the growth process (200 °C). The XPS data also reveal that, at a very high doping level, Fe atoms replace not only III elements but also partly V elements. This is the reason for the use of the III–V:Fe notation instead of (III,Fe)V.

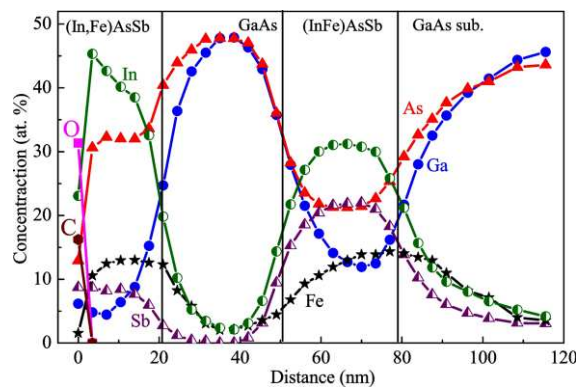


Figure 3. XPS depth distribution profiles of C, O, In, Ga, As, Sb and Fe atoms from the surface to the substrate for sample M1.

Figures 4(a) and 4(b) present overview TEM and HRTEM images of sample M2. All layers of sample M2 can be revealed in the images: the lower InAsSb:Fe layer (ca. 23 nm thick), the GaAs spacer (ca. 20 nm thick) and the upper InGaSb:Fe layer (ca. 23 nm thick). The FFT diffraction pattern (inset to Figure 4(b)) contains spots related to the GaAs regions (the substrate and the spacer layer) and to

the InAsSb:Fe/InGaSb:Fe magnetic semiconductor layers. The InAsSb:Fe and InGaSb:Fe regions give spots that do not differ in the FFT pattern due to the close lattice parameters of these layers.

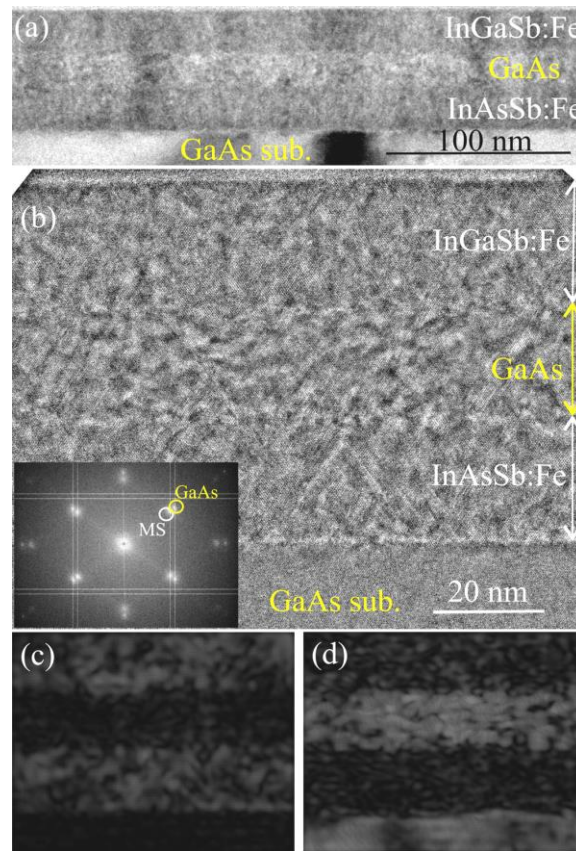


Figure 4. Cross-section TEM images of the InGaSb:Fe/GaAs/InAsSb:Fe/GaAs(sub.) sample M2. (a) Overview TEM image. (b) HRTEM image. The inset shows the respective FFT diffraction pattern. (c) Inverse FFT image of the Fe-doped regions obtained from MS spots. (d) Inverse FFT image of the GaAs regions obtained from GaAs spots.

Figure 5 shows the HRTEM images at a higher magnification in the region of the lower InAsSb:Fe layer (a), in the region of the GaAs spacer (b) and in the region of the upper InGaSb:Fe layer (c). All layers are epitaxial, single-phase and contain microtwins. From the HRTEM images, it was found that the lattice parameters of the InAsSb:Fe layer and the InGaSb:Fe layer differ from that of the GaAs spacer by about 10 % and 8 %, respectively (the lattice mismatch between the GaAs and GaSb single crystals equals 8 %).

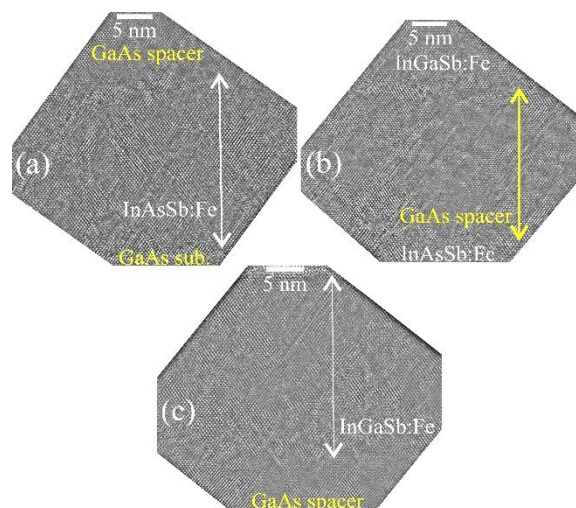


Figure 5. Cross-section HRTEM images of each layer of sample M2. (a) HRTEM image of the lower InAsSb:Fe layer. (b) HRTEM image of the GaAs spacer. (c) HRTEM image of the upper InGaSb:Fe layer.

Figure 6 displays XPS depth profiles of the constituent elements for sample M2. The concentration of Fe atoms in the InAsSb:Fe layer (ca. 17 at. %) and the InGaSb:Fe layer (ca. 23 at. %) is consistent with the nominal Fe content for these layers (Table 1).

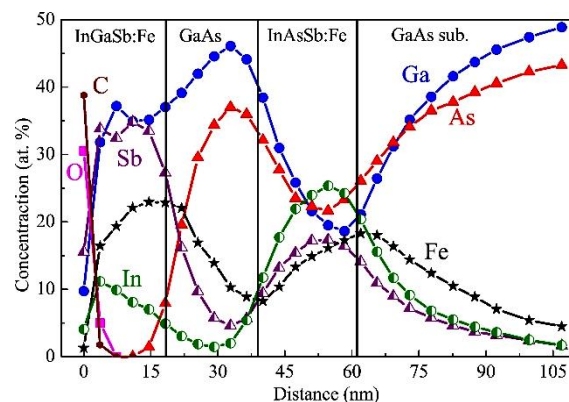


Figure 6. XPS depth distribution profiles of C, O, In, Ga, As, Sb and Fe atoms from the surface to the substrate of sample M2.

As for sample M1, the significant gallium diffusion from the substrate and spacer into the InAsSb:Fe layer occurs in sample M2. A consequence of this is the observation of about 20 at. % Ga in the InAsSb:Fe layer. There is also significant diffusion of Fe atoms in the direction opposite to the growth direction, which leads to the appearance of a significant Fe concentration (ca. 10 at. %) in the GaAs spacer and GaAs substrate.

Figure 7 shows overview and high-resolution cross-section TEM images of sample M3. As for structures M1 and M2, all deposited layers are flat, epitaxial and uniform. The thickness of the lower InGaSb:Fe layer equals ca. 30 nm, that of the GaAs spacer layer is ca. 21 nm and of the upper InSb:Fe layer is ca. 33 nm. The inset of Figure 7(b) shows the FFT diffraction pattern of the whole HRTEM image 7(b). As for structures M1 and M2, the diffraction pattern contains main reflections related to the GaAs regions (substrate and spacer) and the MS layers (InGaSb:Fe and InSb:Fe that have close lattice parameters). Also, the diffraction pattern contains a set of additional spots (denoted as MT) related to microtwins. Figures 7(c) and (d) show inverse FFT images obtained from the main reflexes while Figure 7(e) shows an inverse FFT image obtained from the additional reflexes. Figure 7(e) confirms that the additional diffraction spots correspond to the regions of microtwins that arise in the InGaSb:Fe layer at the boundary with the substrate and grow through all layers to the surface.

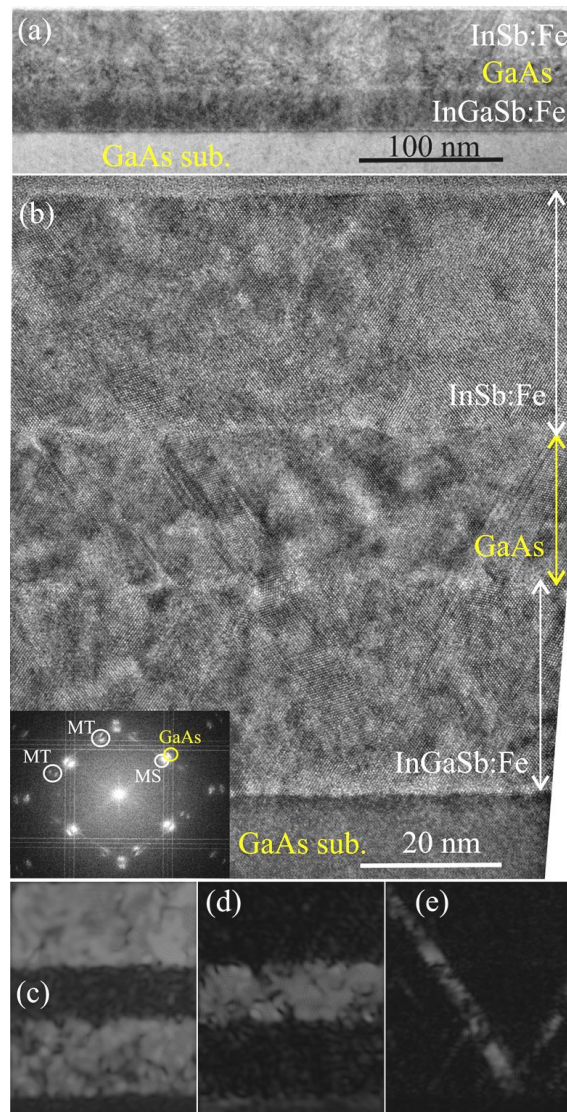


Figure 7. Cross-section TEM images of the InSb:Fe/GaAs/InGaSb:Fe/GaAs (sub.) structure M3. (a) Overview TEM image. (b) HRTEM image. The inset shows the respective FFT diffraction pattern. (c) Inverse FFT image of the Fe-doped regions obtained from MS spots. (d) Inverse FFT image of the GaAs regions obtained from GaAs spots. (e) Inverse FFT image obtained from additional spots.

As for samples M1 (Figure 2) and M2 (Figure 5), all layers of sample M3 have a quite high crystalline quality, do not contain secondary-phase inclusions, and the main defects of the crystal structure are microtwins (Figure 8). From the HRTEM images, it was found that the lattice constants of the InGaSb:Fe layer and the InSb:Fe layers differ from the GaAs spacer lattice constant by about 9 and 13%, respectively.

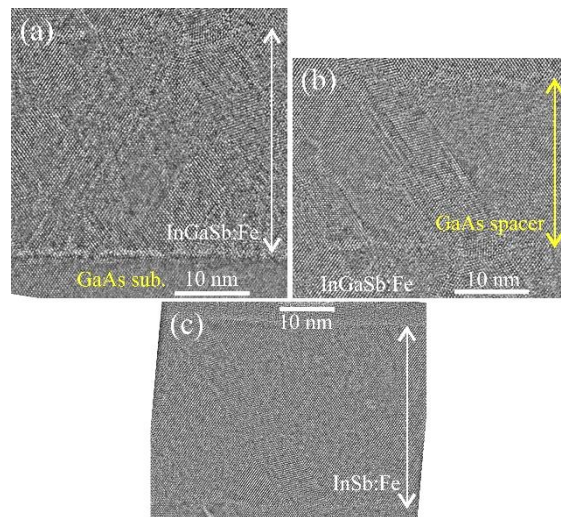


Figure 8. Cross-section HRTEM images of each layer of sample M3. (a) HRTEM image of the lower InGaSb:Fe layer. (b) HRTEM image of the GaAs spacer. (c) HRTEM image of the upper InSb:Fe layer.

Figure 9 shows XPS dependences of the concentration of constituent elements on the distance from the surface for sample M3. The InGaSb:Fe and InSb:Fe layers have a very high Fe concentration (about 20–24 at. %), but despite this, the Fe-doped layers have a rather high crystalline perfection (Figure 8). As for structures M1 (Figure 3) and M2 (Figure 6), significant Fe diffusion into the GaAs spacer and substrate from the Fe-doped layers was revealed for sample M3.

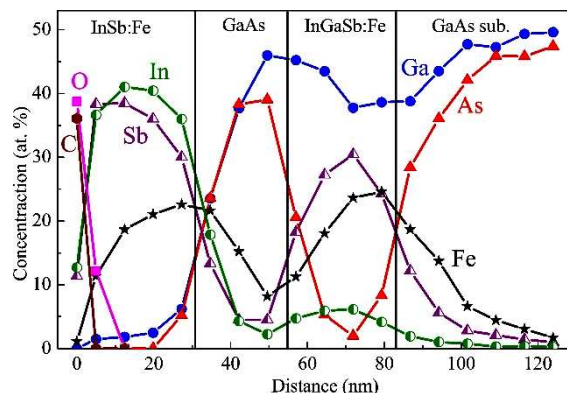


Figure 9. XPS depth distribution profiles of C, O, In, Ga, As, Sb and Fe atoms from surface to substrate for structure M3.

3.2. InAsSb:Fe/GaAs and InGaSb:Fe/GaAs structures

Samples M1, M2, M3 considered above contain layers of III–V solid solutions heavily doped with Fe. According to the HRTEM and XPS data, these multi-component layers are single-phase with a Fe concentration in the range of 13–24 at. %. It is of interest to determine the basic transport and magnetotransport properties of the individual layers of such magnetic semiconductors. For this, the following single InAsSb:Fe and InGaSb:Fe layers with a nominal thickness of 35 nm were formed on i-GaAs (001) substrates at 200 °C:

Sample S1 – a single $\text{InAs}_{0.8}\text{Sb}_{0.2}\text{:Fe}$ layer with a nominal Fe content of 17 at. %.

Sample S2 – a single $\text{InAs}_{0.5}\text{Sb}_{0.5}\text{:Fe}$ layer with a nominal Fe content of 17 at. %.

Sample S3 – a single $\text{In}_{0.2}\text{Ga}_{0.8}\text{Sb}\text{:Fe}$ layer with a nominal Fe content of 20 at. %.

The technological (nominal) composition of the layers was set to be the same as in samples M1, M2 and M3. The structures are listed in Table 2.

Table 2. The investigated single-layer samples and their nominal composition.

Sample	Structure
S1	(InAs _{0.8} Sb _{0.2}) _{0.83} Fe _{0.17} /i-GaAs
S2	(InAs _{0.5} Sb _{0.5}) _{0.83} Fe _{0.17} /i-GaAs
S3	(In _{0.2} Ga _{0.8} Sb) _{0.8} Fe _{0.2} /i-GaAs

Figure 10 presents temperature dependences of the resistivity $\rho(T)$ for samples S1 and S2. Sample S1 with a technological ratio of the Sb and As concentrations equal to 1:4 has a very weak $\rho(T)$ dependence, which is similar to the temperature dependences of the resistivity for MBE-grown (In,Fe)As layers [10]. The $\rho(T)$ dependence for sample S2 with a nominal ratio of the Sb and As concentrations equal to 1:1 is much more pronounced and is similar to the $\rho(T)$ dependences for the PLD-grown InSb:Fe layers [3].

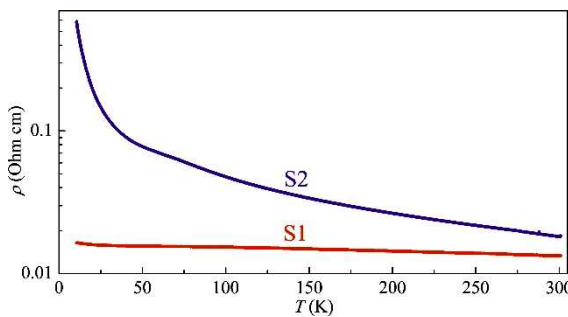


Figure 10. Temperature dependences of the resistivity for samples S1 and S2.

Figure 11 shows Hall resistance dependences in an external magnetic field $R_H(B)$ in the temperature range of 30–130 K for sample S1. For all temperatures, the main contribution to the $R_H(B)$ dependence comes from the ordinary Hall effect corresponding to the n-type conductivity. The concentration and mobility of carriers (electrons) at 300 K obtained from the Hall effect data are about $1 \cdot 10^{19} \text{ cm}^{-3}$ and $40 \text{ cm}^2/(\text{V} \cdot \text{s})$, respectively. The carrier concentration in the obtained InAsSb:Fe layers is determined by the native point defects of the semiconductor matrix, which are predominantly donors in the InAs and InSb semiconductors. At temperatures below 70 K the $R_H(B)$ dependences have also a component related to the anomalous Hall effect (AHE). At 10 K the $R_H(B)$ dependence is hysteretic with saturation in magnetic fields above 0.15 T. The magnitude of the magnetoresistance in sample S1 is small. At temperatures below 70 K, the negative magnetoresistance (NMR) of less than 0.05 % at 0.3 T was observed. The Curie temperature of the InAsSb:Fe layer of sample S1 can be estimated as approx. 40 K, while the Fe concentration is about 15 at. %.

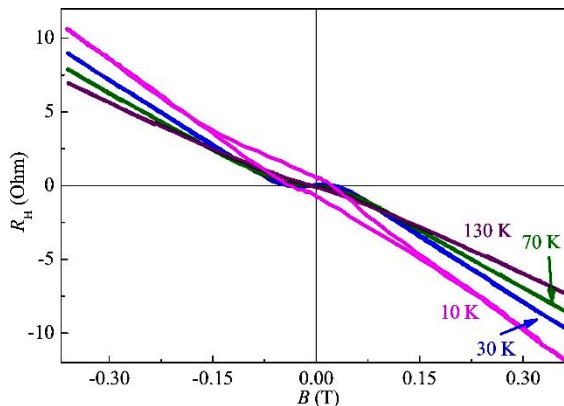


Figure 11. $R_H(B)$ dependences at various temperatures for sample S1.

Figure 12 presents $R_H(B)$ dependences in the temperature range of 30–300 K for sample S2. In contrast to sample S1, the $R_H(B)$ dependences for sample S2 are determined by the anomalous Hall

effect up to at least 300 K. The sign of the $R_H(B)$ curves corresponds to the p-type conductivity, while according to the sign of the Seebeck coefficient, the InAsSb:Fe layer of sample S2 (as well as sample S1) exhibits n-type conductivity. Note that the difference in the sign of the ordinary and anomalous Hall effect was also detected for structure S1 (Figure 11). This is also characteristic of the (In,Fe)As [10] and (In,Fe)Sb layers [3]. Figure 12(b) shows the magnetoresistance curves $MR(B)$ for structure S2 at different temperatures (with the magnetic field applied perpendicularly to the sample plane). A pronounced NMR, hysteretic at temperatures below 200 K, was observed. Thus, in contrast to sample S1, the Curie temperature of the InAsSb:Fe layer of sample S2 is at least 200 K. For sample S2, the $R_H(B)$ and $MR(B)$ dependences are similar to the corresponding dependences for the PLD-grown (In,Fe)Sb layers [3].

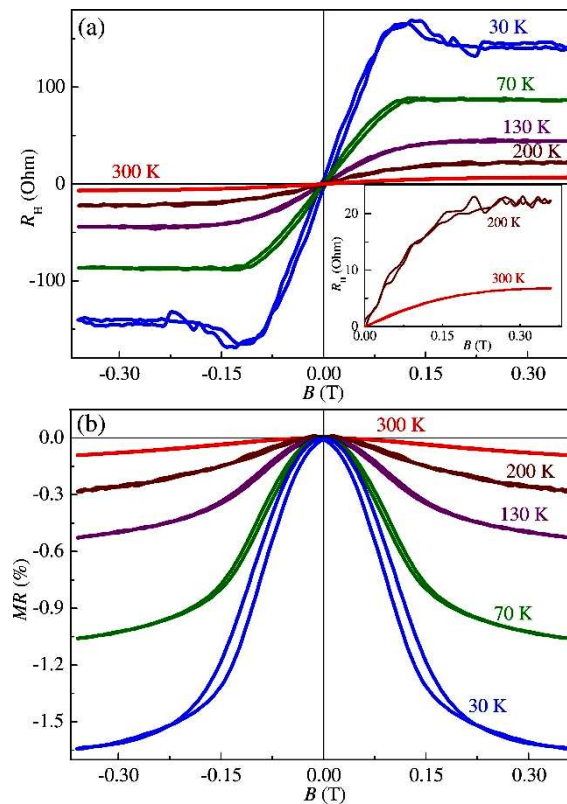


Figure 12. $R_H(B)$ dependences (a) and magnetoresistance (b) at various temperatures for sample S2.

The results obtained for structures S1 and S2 allow us to conclude that the transport and magnetic properties of the InAsSb:Fe layers strongly depend on the ratio of the Sb and As concentrations. The increase in the Sb concentration enhances the ferromagnetic properties (the magnitudes of the AHE, NMR and Curie temperature) of the InAsSb:Fe magnetic semiconductor and (as expected) brings it closer to the properties of the (In,Fe)Sb magnetic semiconductor. The nature of the ferromagnetic exchange interaction in the III-V:Fe magnetic semiconductors is currently the subject of research, and no undisputed opinion can be pointed out. There is the assumption that the ferromagnetism in (In,Fe)As is related to the mechanism of indirect ferromagnetic exchange via charge carriers [10]. At the same time, the magnetic properties of (In,Fe)Sb do not depend on the concentration and type of the majority charge carriers [11] and are probably associated with some mechanism of ferromagnetic exchange consisting in the overlapping of the wave functions of Fe atoms via intermediate atoms (i.e. some kind of superexchange mechanism). The observed enhancement of the magnetic properties of InAsSb:Fe with increasing Sb content indicates that the indirect ferromagnetic exchange interaction between Fe atoms via Sb atoms is stronger than that via As or In atoms.

Figure 13(a) shows $R_H(B)$ dependences in the temperature range of 10–300 K for the InGaSb:Fe layer of sample S3. The anomalous Hall effect dominates the $R_H(B)$ dependences up to at least 300 K.

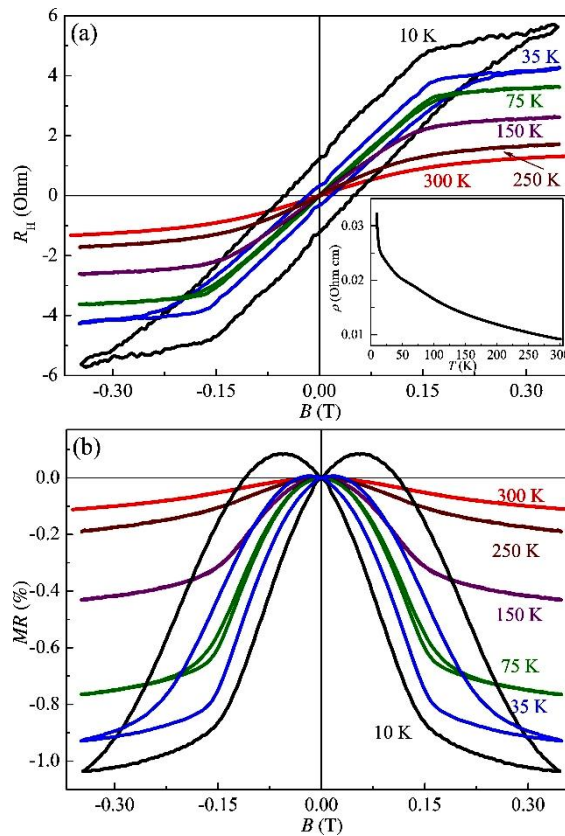


Figure 13. $R_H(B)$ dependences (a) and magnetoresistance (b) at various temperatures for sample S3.

The sign of the $R_H(B)$ curves corresponds to the p-type conductivity, and the sign of the Seebeck coefficient also reveals the p-type conductivity of the InGaSb:Fe layer in sample S3. The p-type conductivity is characteristic of heavily Fe-doped GaSb layers, which is related to native acceptor point defects in the GaSb matrix. In the InGaSb:Fe layer of sample S3, the concentration of In atoms does not exceed 10 at. % (Table 2, Figures 6 and 9). Therefore, the InGaSb:Fe layer should be closer in its properties to the (Ga,Fe)Sb compound. For structure S3, in addition to the anomalous Hall effect, a pronounced NMR at temperatures up to 300 K was also observed (Figure 13(b)). From the Arrott plots of the $R_H(B)$ dependencies, it was concluded that the Curie temperature for the InGaSb:Fe layer of sample S3 is about 300 K.

The presented results allow us to conclude that pulsed laser deposition makes it possible to grow high-quality multilayer epitaxial heterostructures based on various multi-component layers of III-V semiconductors heavily doped with Fe.

4. Conclusions

In summary, using pulsed laser sputtering of solid targets in a vacuum, it is possible to form three-layer epitaxial heterostructures containing layers of various III-V:Fe multi-component magnetic semiconductors, such as InAsSb:Fe and InGaSb:Fe, with a Fe concentration in the range of 13–24 at. %. It has been found that the diffusion of Ga atoms from the GaAs regions leads to the appearance of up to 20 at. % of gallium in layers with the nominal composition InAsSb:Fe, i.e. to the formation of InGaAsSb:Fe layers. It has been established that the ferromagnetic properties (the magnitude of the anomalous Hall effect, negative magnetoresistance and Curie temperature) of the InAsSb:Fe magnetic semiconductor are enhanced with increasing Sb:As ratio. Therefore, we conclude that the indirect ferromagnetic exchange interaction between Fe atoms occurs predominantly via Sb atoms.

Author Contributions: Conceptualization, A.V.K., V.P.L. and N.A.S.; methodology, A.V.K., R.N.K., A.A.Y. and N.Yu.T.; software, A.A.Y.; validation, A.V.K., N.A.S. and M.V.D.; formal analysis, Yu.A.D., M.V.D. and A.V.K.;

investigation, A.V.K., V.P.L., R.N.K., A.A.Y. and N.Yu.T.; resources, V.P.L.; data curation, A.V.K. and N.A.S.; writing—original draft preparation, A.V.K.; writing—review and editing, A.V.K., N.A.S. and M.V.D.; visualization, A.V.K.; supervision, A.V.K., N.A.S. and Yu.A.D.; project administration, A.V.K. and M.V.D.; funding acquisition, N.A.S. and M.V.D. All authors have read and agreed to the published version of the manuscript.

Funding: This study was supported by the Russian Science Foundation (grant № 21-79-20186, magnetotransport measurements) and the project i3N, UIDB/50025/2020, and UIDP/50025/2020 which was financed by national funds through the Fundação para a Ciéncia e Tecnologia (FCT) and the Ministério da Educação e Ciéncia (MEC) of Portugal (data analysis).

Conflicts of Interest: The authors declare no conflict of interest.

References

1. Tu, N.T.; Hai, P.N.; Anh, L.D.; Tanaka, M. High-temperature ferromagnetism in heavily Fe-doped ferromagnetic semiconductor (Ga,Fe)Sb. *Appl. Phys. Lett.* **2016**, *108*, 192401-4. <https://doi.org/10.1063/1.4948692>
2. Danilov, Yu.A.; Kudrin, A.V.; Lesnikov, V.P.; Vikhrova, O.V.; Kryukov, R.N.; Antonov, I.N.; Tolkachev, D.S.; Alaferdov, A.V.; Kun'kova, Z.E.; Temiryazev, M.P.; Temiryazev, A.G. The Study of Features of Formation and Properties of A³B⁵ Semiconductors Highly Doped with Iron. *Phys. Solid State* **2018**, *60*, 2178-2181. <https://doi.org/10.1134/S1063783418110033>
3. Kudrin, A.V.; Danilov, Yu.A.; Lesnikov, V.P.; Dorokhin, M.V.; Vikhrova, O.V.; Pavlov, D.A.; Usov, Yu.V.; Antonov, I.N.; Kriukov, R.N.; Alaferdov, A.V.; Sobolev, N.A. High-temperature intrinsic ferromagnetism in the (In,Fe)Sb semiconductor. *J. Appl. Phys.* **2017**, *122*, 183901-8. <https://doi.org/10.1063/1.5010191>
4. Tu, N.T.; Hai, P.N.; Anh, L.D.; Tanaka, M. High-temperature ferromagnetism in new n-type Fe-doped ferromagnetic semiconductor (In,Fe)Sb. *Appl. Phys. Express* **2018**, *11*, 063005 (1-4). <https://doi.org/10.7567/APEX.11.063005>
5. Kudrin, A.V.; Lesnikov, V.P.; Danilov, Yu.A.; Dorokhin, M.V.; Vikhrova, O.V.; Demina, P.B.; Pavlov, D.A.; Usov, Yu.V.; Milin, V.E.; Kuznetsov, Yu.M.; Kriukov, R.N.; Konakov, A.A.; Tabachkova, N.Yu. High-temperature intrinsic ferromagnetism in heavily Fe-doped GaAs layers. *Semicond. Sci. Technol.* **2020**, *35*, 125032 (1-13). <https://doi.org/10.1088/1361-6641/abbd5c>
6. Kudrin, A.V.; Lesnikov, V.P.; Pavlov, D.A.; Usov, Yu.V.; Danilov, Yu.A.; Dorokhin, M.V.; Vikhrova, O.V.; Milin, V.E.; Kriukov, R.N.; Kuznetsov, Yu.M.; Trushin, V.N.; Sobolev, N.A. Formation of epitaxial p-i-n structures on the basis of (In,Fe)Sb and (Ga,Fe)Sb diluted magnetic semiconductors layers. *J. Magn. Magn. Mater.* **2019**, *487*, 165321 (1-6). <https://doi.org/10.1016/j.jmmm.2019.165321>
7. Tu, N.T.; Otsuka, T.; Arakawa, Y.; Anh, L.D.; Tanaka, M.; Hai, P.N. Spin transport in fully ferromagnetic p-n junctions. *J. Appl. Phys.* **2022**, *131*, 013902 (1-14). <https://doi.org/10.1063/5.0072128>
8. Hotta, T.; Takase, K.; Takiguchi, K.; Sriharsha, K.; Anh, L.D.; Tanaka, M. Growth and characterization of quaternary-alloy ferromagnetic semiconductor (In,Ga,Fe)Sb. *AIP Adv.* **2022**, *12*, 015307 (1-6). <https://doi.org/10.1063/5.0069282>
9. Briggs, D.; Seah, M.P. *Practical surface analysis by Auger and X-ray photoelectron spectroscopy*, 3rd ed.; John Wiley and Sons Ltd., 1990.
10. Hai, P.N.; Anh, L.D.; Mohan, S.; Tamegai, T.; Kodzuka, M.; Ohkubo, T.; Hono, K.; Tanaka, M. Growth and characterization of n-type electron-induced ferromagnetic semiconductor (In,Fe)As. *Appl. Phys. Lett.* **2012**, *101*, 182403 (1-5). <https://doi.org/10.1063/1.4764947>
11. Kudrin, A.V.; Lesnikov, V.P.; Danilov, Yu.A.; Dorokhin, M.V.; Vikhrova, O.V.; Pavlov, D.A.; Usov, Yu.V.; Antonov, I.N.; Kriukov, R.N.; Zubkov, S.Yu.; Nikolichev, D.E.; Konakov, A.A.; Dudin, Yu.A.; Kuznetsov, Yu.M.; Temiryazeva, M.P.; Sobolev, N.A. Robustness of ferromagnetism in (In,Fe)Sb diluted magnetic semiconductor to variation of charge carrier concentration. *J. Magn. Magn. Mater.* **2019**, *485*, 236-243. <https://doi.org/10.1016/j.jmmm.2019.04.088>

Disclaimer/Publisher's Note: The statements, opinions and data contained in all publications are solely those of the individual author(s) and contributor(s) and not of MDPI and/or the editor(s). MDPI and/or the editor(s) disclaim responsibility for any injury to people or property resulting from any ideas, methods, instructions or products referred to in the content.